Degradation of High-Voltage Solar Array Due to Arcing in Plasma Environment

著者	Toyoda Kazuhiro, Okumura Teppei, Hosoda Satoshi, Cho Mengu
journal or publication title	Journal of Spacecraft and Rockets
volume	42
number	5
page range	947-953
year	2005-09
その他のタイトル	Degradation of High Voltage Solar Array due to Arcing in LEO plasma Environment
URL	http://hdl.handle.net/10228/00007489

doi: info:doi/10.2514/1.11602

JOURNAL OF SPACECRAFT AND ROCKETS
Vol. 42, No. 5, September–October 2005

Degradation of High-Voltage Solar Array Due to Arcing in Plasma Environment

Kazuhiro Toyoda*
Chiba University, Chiba 263-8522, Japan
and
Teppei Okumura,† Satoshi Hosoda,‡ and Mengu Cho§
Kyushu Institute of Technology, Kitakyushu 804-8550, Japan

A degradation test for a solar array coupon against electrostatic discharge was performed under a simulated low-Earth-orbit environment as part of research project to develop the next-generation 400-V high-voltage solar array technology. All tests were performed in a vacuum chamber with a plasma source. An inductance–capacitance–resistance circuit was used to simulate the arc current that would flow by collecting electric charge stored on cover glasses. Arcs were repeated until the solar array coupon showed degradation of electrical output. The locations, current waveform, and voltage waveforms of all the arcs during the tests were recorded. The electrical output of the coupon was measured without opening the vacuum chamber. The arc that damaged a solar cell was identified; the cell was damaged by only one arc, which occurred at the edge of the cell.

I. Introduction

RECENT spacecrafts have larger structures and longer lifetimes and need a large amount of electric power generation, often larger than 10 kW. The International Space Station (ISS) generates 65 kW of electric power. The higher bus voltage is necessary for the large spacecraft to reduce the power line weight and the power loss due to Joule heating as the generated power increases. The bus voltage of 100 V or higher is employed for 10-kW-class spacecraft and the output voltage of the solar array of such spacecraft is higher than 100 V. In the case of the ISS, electric power is generated at a voltage of 160 V and transmitted at 120 V. In the near future, the electric power will increase further as much larger spacecraft appear, such as a space factory, a space hotel, or an experimental solar power satellite, that will use power of 1 MW or more. Considering the fact that the bus voltage should be proportional to the square root of the electric power, the 1-MW-class spacecraft will need an output voltage of about 400 V.

The negative end of the solar array is usually connected to the spacecraft body. In the low-Earth-orbit (LEO) environment, space plasma, the density of which is of the order of 10^{10}–10^{12} m^{-3}, can charge a spacecraft to a negative potential with respect to the plasma due to the high mobility of electrons. The spacecraft potential also depends on plasma parameters and spacecraft design. If the positive end of the solar array has the same potential as the ambient plasma, the spacecraft body and the negative end of the solar array have negative potential equal to the output voltage. In this case, the solar array generates power at 400 V, most of the spacecraft circuit and the solar array have negative potentials with respect to the plasma, and the negative end of the solar array is −400 V.

Arcing is observed on the spacecraft surface, especially the solar array, when a spacecraft has a negative potential of over 250 V with respect to the ambient plasma.[1] An arc occurs on the solar array surface as the potential difference between surface insulator (such as cover glass, adhesive, or insulator film) and the spacecraft chassis (such as an interconnector) exceeds about 200 V. A cross-sectional view of a typical spacecraft solar array is shown in Fig. 1. The solar cells are glued on insulator substrate (usually made of polyimide film) by adhesive and are connected in series with each other by the interconnectors (conductor). The cover glasses are also glued on the cells. When the spacecraft has a negative potential with respect to the ambient plasma, some cells and interconnectors also have negative potentials. Therefore, positive ions are attracted to the cells and charge the cover glasses. This potential difference between the cover glass and the interconnector enhances the electric field at the triple junction, which consists of the interconnector, the cover glass, and the plasma. The electrons emitted by field emission from the triple junction collide with the side surface of the cover glass. The electric field is enhanced further by charging of the cover glass, leading to an avalanche of electron emission and ionization of desorbed gas.[2]

The arcing causes degradation of solar cells, malfunction of electrical devices, and short circuit of solar array circuit. The degree of influence of the arcs depends on both the number and the energy of the arcs. The more negatively the spacecraft is charged, the higher the arc rate becomes. The arc energy is supplied by the electrostatic energy stored in the dielectric material, such as the cover glass, near the arc spot. Therefore, the arc energy also becomes larger as the voltage becomes higher.

There have been research efforts to develop 300- or 400-V high-voltage solar arrays in LEO plasma environment.[3–5] There are several mitigation methods that are very promising to suppress arc inception. No mitigation method, however, is a perfect solution to suppress arcing. Covering the solar array surface with a sheet of transparent film can suppress arc inception up to 1000 V (Refs. 3 and 4). Debris or meteoroid impact may punch a hole in the film, jeopardizing the effectiveness. Using room-temperature vulcanizing (RTV) grouting sometimes works, but a void in the adhesive often becomes an arc spot. A wrap-through cell like the one used in ISS is also effective, but arcs can occur at the exposed triple junction formed at the edge of the solar cells. The arcs occurring at cell edges can cause damage to cells. Therefore, to develop 400-V space photovoltaic technology, we need to consider not only suppressing arc inception but also minimizing the damage caused by each arc.

In previous work,[6] we found that arcing may damage the solar cell positive–negative (PN) junction. The damage is not as extensive as the so-called sustained arc,[7] which destroys one or more strings of a solar array circuit. An arc that ends as a single pulse of current, the

Received 16 June 2004; revision received 17 August 2004; accepted for publication 26 August 2004.

*Research Associate, Department of Urban Environment Systems; toyoda@tu.chiba-u.ac.jp. Member AIAA.
†Graduate Student, Department of Electrical Engineering.
‡Postdoctoral Fellow, Satellite Venture Business Laboratory.
§Associate Professor, Department of Electrical Engineering, 1-1 Sensui, Tobata; cho@ele.kyutech.ac.jp. Member AIAA.

so-called trigger arc, may destroy only one cell or contaminate the coverglass surface by outgassing. The purpose of the present paper is to investigate the mechanism of PN-junction damage caused by a trigger arc in detail via a laboratory experiment in simulated LEO plasma environment. We investigate what type of arc damages the PN junction and estimate the tolerance limit to which we can allow in the operational lifetime of a given spacecraft. Knowing the tolerance limit will give us a goal of how far we should suppress arc inception.

In the second part of this paper, we describe the experimental system that has been developed for the present purpose. We have developed systems that can record all the arc current waveforms and identify all the arc inception locations. By matching the waveform and the arc location, we can identify characteristics of the arcs that destroy the PN junction. In the third part, we present the experimental results and discuss the tolerance limit for real spacecraft. In the fourth part, we conclude the paper with suggestion of future work.

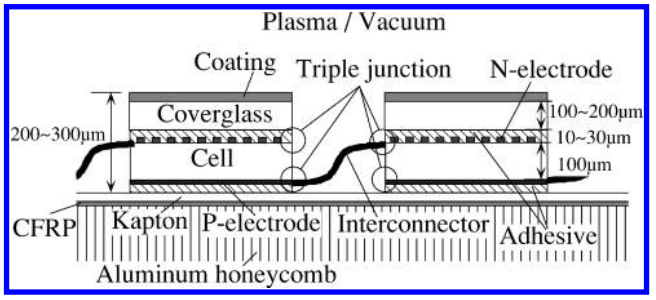

Fig. 1 Cross section of a solar array.

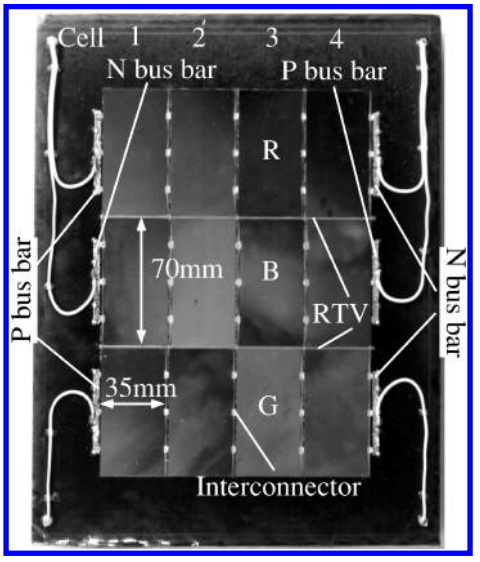

Fig. 2 Picture of the solar array coupon.

II. Experiment

A. Solar Array Coupon

The solar array coupon used in the experiments is shown in Fig. 2. This coupon uses a standard design of a typical 100-V satellite that is currently in use. The substrate is 25-mm-thick aluminum honeycomb which is covered with carbon-fiber-reinforced plastic, and the top of the substrate is covered with Kapton® film. The 12 silicone cells (70 mm × 35 mm) are glued on the Kapton film. Four cells are connected in series via interconnectors. The electrodes connected to the end of the series connection are called bus bars. In the present paper, we call the bus bars and the interconnectors "exposed electrodes" and call the side edges of cells "cell edges." The cell edge contains two types of the triple junctions. One is formed by a P-electrode and the adhesive between a cell and insulator substrate. The other is formed by an N-electrode and adhesive between a cell and cover glass. Both the triple junctions, especially the N-electrode, are not necessarily exposed to the ambient plasma.

Three parallel connections are denoted strings R, B, and G, respectively. We designate each cell on the coupon by the number shown in Fig. 2. We also call the cells by the numbers shown in Fig. 2. The cells have an integration bypass function (IBF), which allows the current flow from N to P electrodes in the cell even if the cells cannot generate the electric power. The gap between strings is glued by RTV silicone rubber to prevent the sustained arc.[8,9] The coupon was kept at 40°C by an infrared (IR) lamp during the experiment to simulate the temperature on orbit. We biased the coupon to 400 V by a dc power supply.

The coupon we used is a new coupon that was not used for any previous experiment. After it was shipped from a factory, it was left in an ordinary laboratory room without any humidity control. Although the coupon temperature was kept at 40°C during the experiment, no baking was done before the experiment. From these facts, the coupon is likely to have a very high arc rate at the beginning of experiment, because the surface contains much water vapor and many contaminant particles that provoke arc inception.

B. Experiment System

A schematic picture of the experimental system is shown in Fig. 3. The experiments were performed in a vacuum chamber, which was 1 m in diameter and 1.2 m in length. The pressure in the chamber

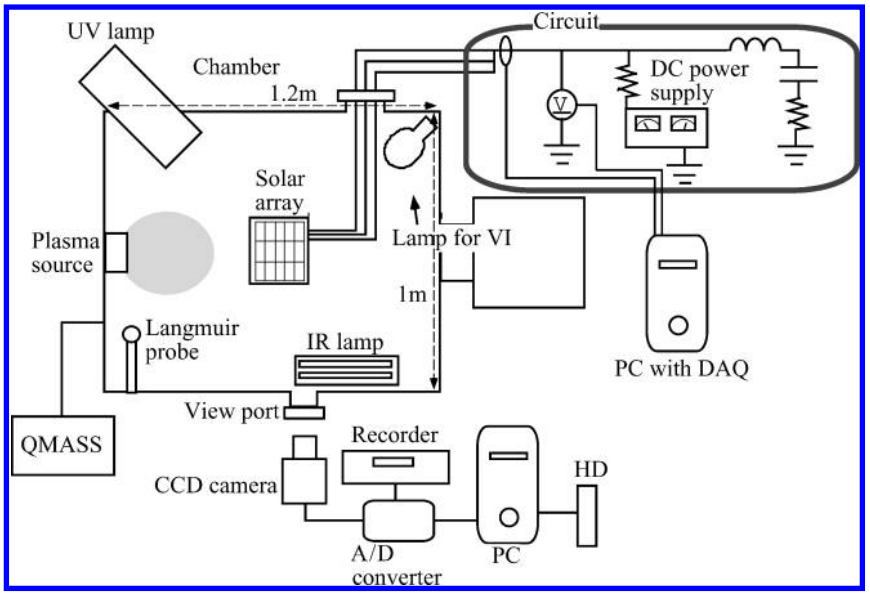

Fig. 3 Experimental system.

was 9.7×10^{-3} Pa during the experiments. Plasma was produced by an electron cyclotron resonance plasma source[10] with xenon as the working gas. The plasma density around the coupon was about 2×10^{12} m^{-3} and the electron temperature was about 3–7 eV with xenon gas flow rate of 2×10^{-8} kg/s.

The arc location on the coupon was identified by the arc position identification system.[11] During the experiments, video image of the coupon was recorded to a hard disk drive connected to a personal computer. After the experiments, the arc location was identified automatically by analyzing the digital video image with a computer program on the personal computer.

All waveforms of both the array potential and the arc current were acquired by a high-speed data acquisition system.[12] This system consists of a high-speed data acquisition board, a personal computer, and the LabVIEW® program. This system can record the waveforms of each arc in as short as 30-ms intervals. The circuit used in the experiments is shown in Fig. 4. The derivation of the external circuit is discussed in detail in the Appendix. The numbers of L, C, and R were chosen so that the arc current waveform generally has the shape shown in Fig. 5. The current probes CP1 and CP2 can measure from dc to 10 MHz. The current supplied from the external capacitance, C ($=5\ \mu$F), was measured as the voltage drop of a pickup resistance of 0.1 Ω using a differential voltage probe.

The metal halide lamp installed inside the chamber enables us to measure the electrical performance of the coupon without opening the chamber during the experiments. A circuit with variable resistors was connected to the coupon for electrical performance measurement. The electrical performance was measured in each string by varying the value of resistance connected to the string. An example plot of the voltage-current (VI) characteristic of a string before the experiment is shown in Fig. 6. The output power is also shown. The light intensity of this lamp was 19,000 lx at the center of the coupon. The plasma source was turned off during the VI measurement. The VI curve was corrected by the coupon temperature, which was measured simultaneously, because the electric performance of the solar cell depended on its temperature.

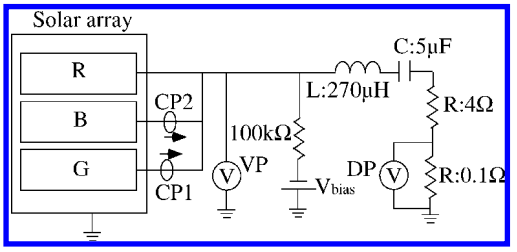

Fig. 4 Schematic picture of external circuit with LCR.

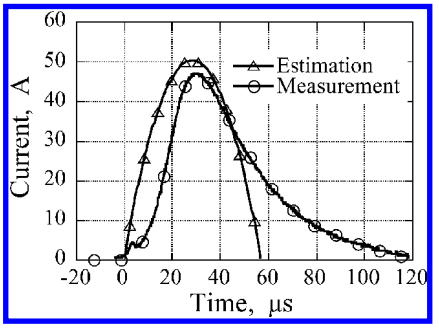

Fig. 5 Typical waveform of arc current supplied by the external circuit shown in Fig. 4.

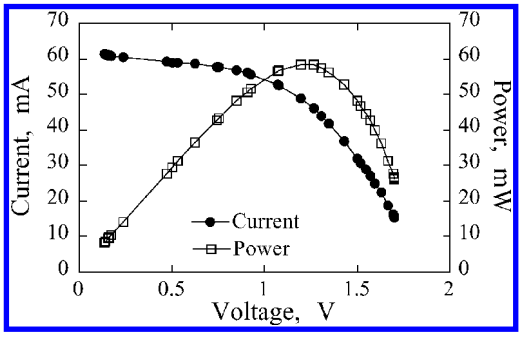

Fig. 6 Result of VI characteristic measurement.

III. Results and Discussion

Table 1 lists the experimental result. The coupon was biased at −400 V in the plasma environment. Each experimental case was repeated until the coupon was degraded. After each experimental case, the VI characteristic was measured. By the end of the experiment, the coupon had been exposed to the plasma with 400 V bias for 565 s and suffered 295 arcs. Among the 295 arcs, 269 arcs occurred at the exposed electrodes and 26 arcs occurred at the cell edge. This result indicates that arcs occurred more easily at the exposed electrode than at the cell edge. From this table, the average arc interval was 1.9 s/arc. Capacitor charging time is about 1.5 s. Therefore, because the arc interval was close to the charging time, some arcs occurred before the capacitor was fully charged.

The peak of the output electric power measured after every case is shown in Fig. 7. The maximum power P_{max} was normalized by the value measured before the experiment. The maximum power did not change in any strings until case 5. In case 6, string R showed degradation of electric power. In case 9, string G suffered the degradation by 20%, and suffered 20% more degradation after case 10. By the end, the total power degradation was 40% in string G. String B showed little degradation.

In Fig. 8, we show the VI characteristics of string G after the experiment. This measurement was performed under atmospheric condition after the coupon was removed from the vacuum chamber. Degradation appears mainly as a decrease in the open circuit voltage V_{oc}, indicating that short circuit via formation of a leak resistance occurred somewhere in the string. We measured V_{oc} of each cell in string G by exposing one cell to the light while shading the other cells. We found that V_{oc} of cells 1 and 2 decreased by 90% after the experiment.

The arcs occurred at the side edge of the cells in both string G and string R when the electric power decreased. In Fig. 9 we show the distributions of the arc location. In string G, arcs at the cell edge did

Table 1 Number of arcs

Case	Experimental duration, s	Number of arcs	Electrode	Cell edge
1	100	53	53	0
2	62	29	29	0
3	26	18	18	0
4	40	28	26	2
5	39	25	23	2
6	78	41	38	3
7	37	18	18	0
8	76	34	30	4
9	55	26	19	7
10	52	23	15	8
Total	565	295	269	26

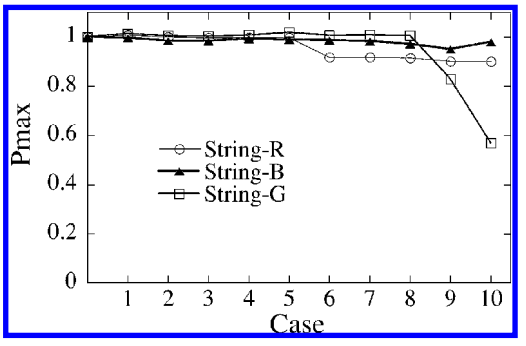

Fig. 7 Peak value of output power measured after each case: the values are normalized by the value before experiment.

not occur until case 8. The electrical output of string G decreased only after case 9. In string R, the electrical output decreased after case 6, where three arcs occurred at cell edges. String B suffered arcs at cell edges in case 8 but showed no power degradation.

Figure 10 shows the microscope photographs of cells that had arcs at their side edges. Cell-edge positions were denoted as a–f. We see that P and N electrodes were melted and left traces of intensive arc currents. The arc locations of the exposed electrode showed little sign of arcs.

At most of the arc locations at the cell edge, it looks as if the cell was connected to the adjacent cell via the arc track. If the P electrodes of the backside of the cells short-circuit each other, the P and N electrodes are short-circuited in one cell and this leads to a decrease in electric power. The resistance between the adjacent cells, cells 1 and 2 in string G, was measured to clarify whether the two cells were short-circuited or not. The three interconnectors connecting two cells were cut to measure the resistance. The result showed that the insulation was maintained between the two cells. From this result, the decrease in electric power resulted from a leak resistance within each cell.

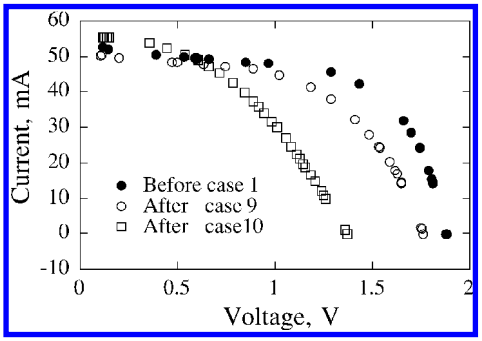

Fig. 8 VI characteristic of string G.

When a leak resistance is inserted within a solar cell, the generated voltage collapses because the generated pairs of an electron and a hole recombine through the leak resistance. When we apply inverse voltage to a solar cell under dark condition, the current flows through the IBF and the leak resistance. Joule heating of the leak resistance causes thermal emission. By detecting IR radiation, we can identify the current leakage point. The current leakage points in cells 1 and 2 of string G were identified in this way. Figure 11 shows microscope photographs of the current leakage point of the cell 2. The left-hand photograph shows IR emission from the leak resistance. The IR signal was emitted from the arc track attached to the N electrode below the cover glass. The arc that produced this arc track was the 264th arc. The cover glass was peeled from the cell to observe the arc track in detail in the right-hand photograph. The track ran on the silicone to the N electrode via melting the silicone. The N^+ diffusion layer of the silicone under the arc track is only 0.1 μm in depth. This layer can be easily destroyed by the arc track.

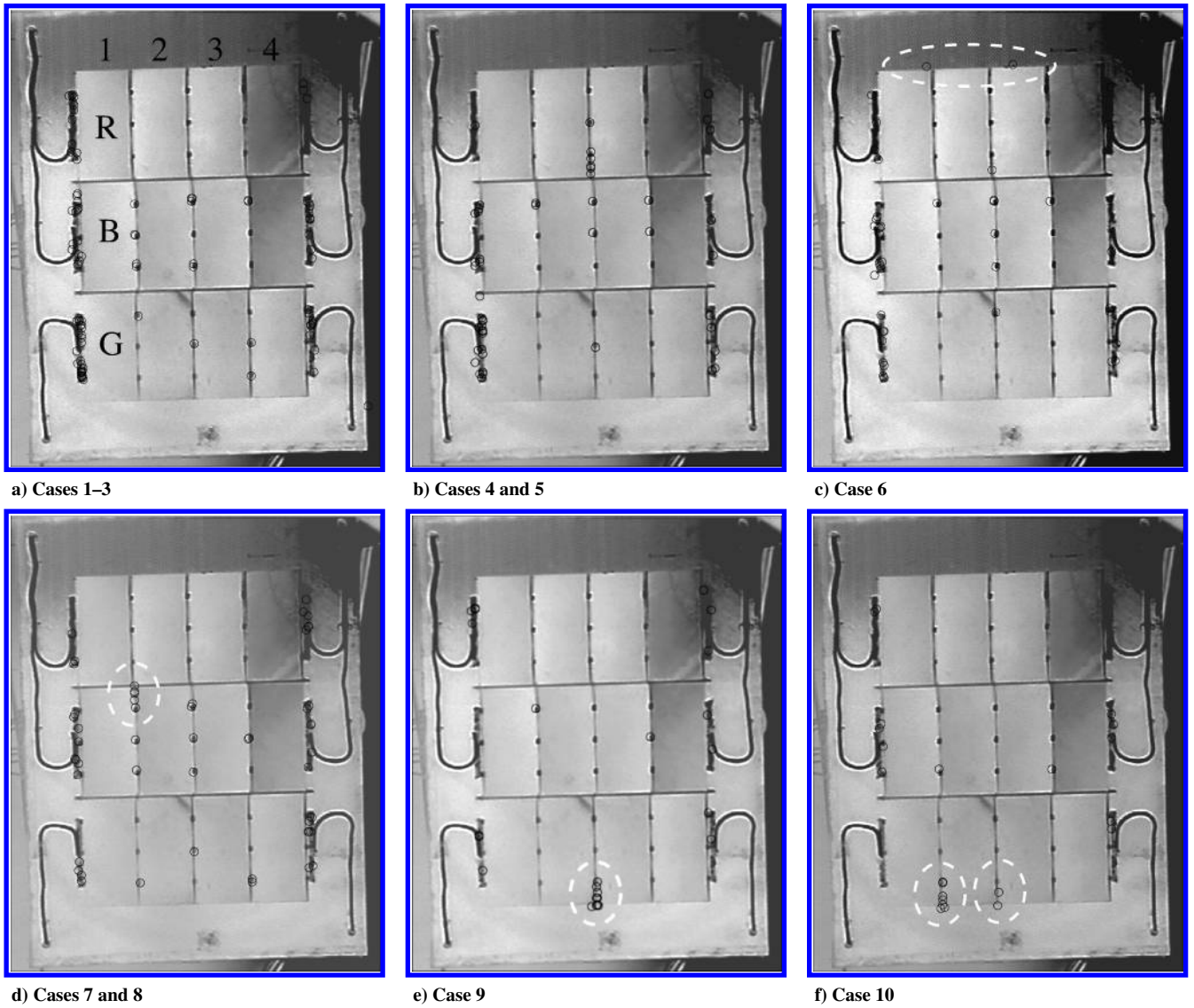

a) Cases 1–3 **b) Cases 4 and 5** **c) Case 6**

d) Cases 7 and 8 **e) Case 9** **f) Case 10**

Fig. 9 Position of arcs.

The current leakage point in cell 1 is marked in Fig. 10d. The current leak occurs at the arc track attached to the N electrode also in this cell; this was produced by the 293rd arc. A simillar arc track was also observed on the current leakage point in cell 2. The arcs that produced the leak resistances were only single arcs for both cell 1 and cell 2. We can conclude that even a single arc can destroy one solar cell.

As shown in Fig. 10a, string R has an arc track attached to the N electrode that coincides with power degradation observed after case 6. Therefore, this arc track is strongly suspected of producing the leak resistance. On the other hand, string B has no such arc track. String B had several arcs at the cell edge in case 8 but did not suffer power degradation. The arc traces in string B are connected only to the P electrode. Therefore, an arc that occurs at the triple junction involving the N electrode has a high probability of producing the leak resistance within a solar cell. We can exclude the possibility of leak resistance formation for arcs at the exposed electrode. It is still premature, however, to exclude the possibility for arcs at the P electrode. We need more experimental evidence that arcs appearing at the N electrode is the necessary condition for the power degradation.

The current waveforms of the 264th and 293rd arcs that produced the leak resistance in cells 1 and 2 of string G are shown in Fig. 12. The current waveform was measured by the current probe CP1 in the circuit (Fig. 4). The overall shape of the current waveforms is not different from the typical waveform shown in Fig. 5, which is mostly determined by the external LCR circuit. As we look at the waveform in Fig. 12 closely, however, the details differ depending on where the arc occurs.

In Fig. 13 we show the definitions of array potential just before arc inception, V_0, peak of arc current, I_{peak}, arc resistance R_{arc}, and arc power P_{arc}. Figure 14 shows the relationship between the array potential V_0 and the peak current I_{peak}. We put different marks depending on the arc location to distinguish the arcs that occurred at the exposed electrode and the arcs that occurred at the cell edges. Because arcs occurred very frequently in this experiment, recharging of the external capacitance to 400 V did not catch up each arc. Some arcs occurred before the array potential recovered to −400 V. Therefore, the array potential before arc inception, V_0, has various values. The charge stored in the external capacitance before arc inception, Q_0, is proportional to the array potential $|V_0|$. The peak current I_{peak} is generally proportional to the charge Q_0. For the case

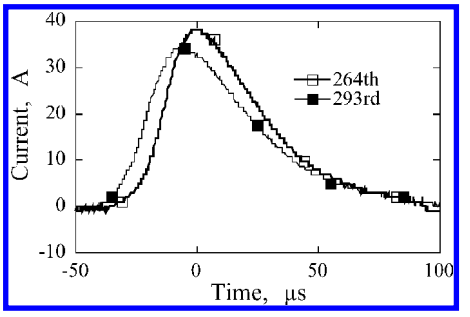

Fig. 12 Waveforms of the arc current that degraded cells 1 and 2 of string G.

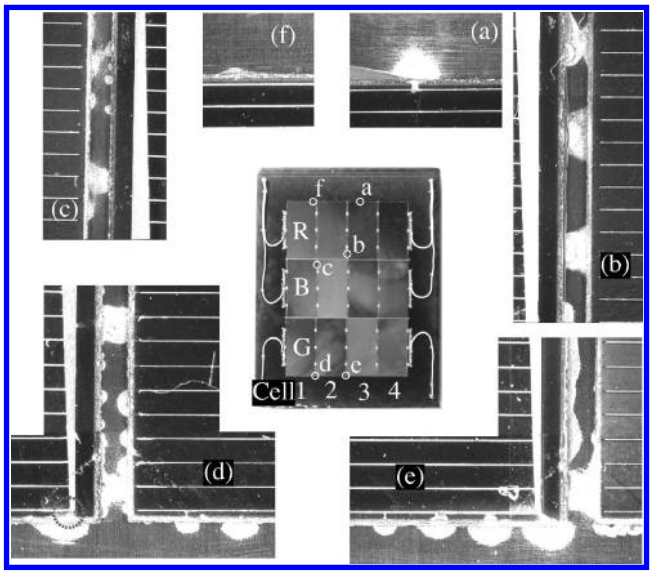

Fig. 10 Microscopic photographs at the cell edges.

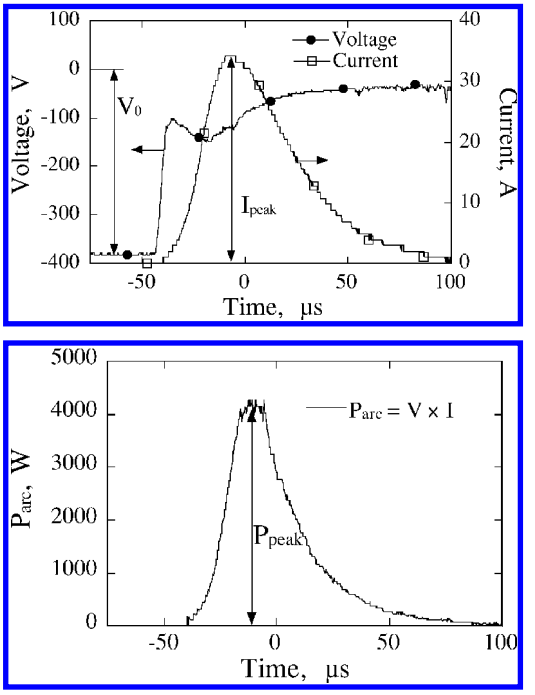

Fig. 13 Definitions of V_0, I_{peak}, and P_{arc}.

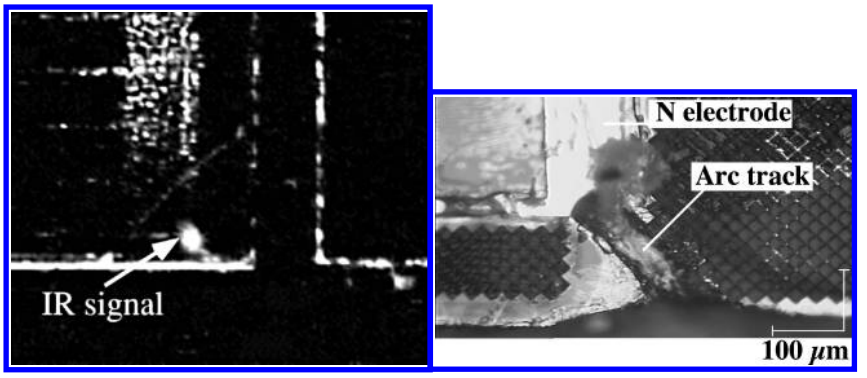

Fig. 11 Current leakage point of cell 2 in string G.

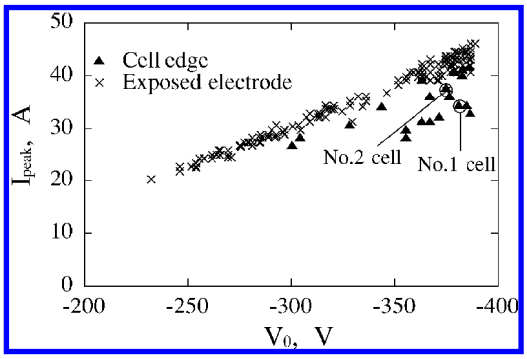

Fig. 14 Relationship between I_{peak} and V_0.

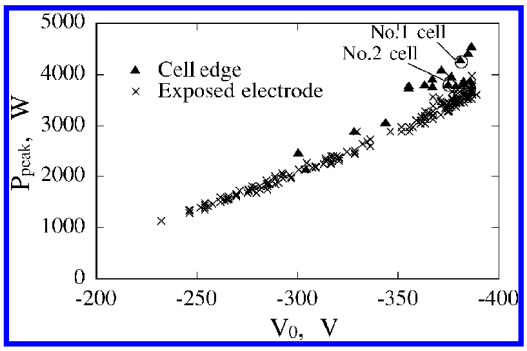

Fig. 15 Relationship between P_{peak} and V_0.

of the arcs at the exposed electrodes, the peak current was proportional to $|V_0|$ and lay on a single line. On the contrary, the peak current of the arcs at the cell edge scatters below the single line.

In Fig. 15, the peak value of P_{arc}, P_{peak} was plotted against V_0. The power P_{arc} injected into the arc plasma was calculated by multiplying the current and the absolute value of the array potential. As shown in Fig. 15, P_{peak} of the cell-edge arcs was larger than that of the electrode arcs. This is because that the voltage drop at the current peak for the cell-edge arcs was higher than that for the electrode arcs. These results suggest that arcs at the cell edge cause concentration of the arc current to a small spot and give excessive heating at the arc spot, which probably led to formation of the leak resistance. On the other hand, the arcs at the exposed electrode give a smaller power density. Even if an arc occurs at the exposed electrode, the heat can be diffused easily by conduction.

We now estimate how much degradation would occur in space. The array was biased at −400 V in the experiment. The power degradation was 10% in string R and 40% in string G. Each string had four cells. Therefore, the loss is equivalent to the loss of two cells. During the experimental time of 565 s, we had 295 arcs. Therefore, the arc rate is 0.52 arc/s. This arc rate is extremely high. We tested two other coupons with exactly the same design. At −400 V, the arc rates were 0.03 and 0.01. From this result, the probability of one arc destroying one cell was about 0.7%. Limiting the arcs at the cell edges, 26 arcs occurred. One cell was destroyed after 7 arcs, two cells after 18 arcs or 26 arcs. The probability of one arc at the cell edge destroying one cell was higher: about 10%. Because of the way solar arrays are designed, loss of a cell may mean loss of up to an entire string, which would greatly amplify the rate of power degradation.

We calculated the arc rate to keep the cell loss under 1% of all the cells. The total hours of sunlight in the satellite lifetime, 10 years, is about 50,000 h. About 20,000 cells, of size 70 mm × 35 mm, are mounted within an area of 4 m in radius. If 200 cells are degraded for 10 years, power degradation is about 1%. The number of arcs degrading 200 cells is $(200 \times 295)/2 \simeq 30{,}000$. Therefore, we should keep the total number of arcs below 30,000, within an area defined by a circle of 4 m radius. The arc rate to cause 1% power degradation is 30,000/50,000 = 0.6 arc/h. From this result, we must suppress the arc rate under 0.6 arc/h. This arc rate is equivalent to 1.7×10^{-4} arc/s, which is smaller than the arc rate of the ground experiment, 0.52 arc/s, by three orders of magnitude. Although 0.52 arc/s can be regarded as the upper bound of the arc rate, we still need to suppress the arc rate significantly. Also, because the cell-damaging arc is limited to the cell edge, we need to keep the arc rate at the cell edge as low as possible.

IV. Conclusions

An electrostatic discharge test of the 400-V power generation solar array for space use was performed in a vacuum chamber simulating the LEO plasma environment. The waveform of arc current was controlled using an inductance–capacitance–resistance (LCR) circuit simulating the neutralization current of coverglass charge. The system that can record all the arc current waveforms, identify all the arc locations, and measure the electrical performance of the solar array in situ was constructed.

Many arcs occurred on the solar array biased at −400 V and degraded the electric performance of the solar array. The degradation appeared as a drop of the open-circuit voltage, indicating formation of a leak resistance within a cell. By identifying the degraded cells and the current leakage point, it was found that a single transient arc destroyed a cell. The interconnector and the bus bar had little damage due to arcing. On the other hand, because the arcs occurred at the cell edge, P and N electrodes melted out. Arc tracks attached to the N electrode were found at the current leakage point. Arcs at the cell edge give excessive heat stress that is locally confined to P or N electrodes and eventually destroy the cell.

Extrapolating the numbers obtained in the ground experiment to 1-MW spacecraft, the limit on the arc rate to keep the power loss below 1% in 10 years was derived to be 0.6 arc/h, which is a significant challenge. By developing a mitigation method to specifically suppress arc inception at the cell edge, this limit can be relaxed.

In the present paper, we have found that cell degradation occurs once an arc track is formed to the N electrode, not to the P electrode. We need to accumulate more experimental data to conclude that the arc track to the N electrode is the necessary condition of cell degradation. We also need to find out the threshold values of arc current, energy, and so on for the cell degradation to occur.

Appendix: Charge Supplied by the Charged Cover Glass

In this Appendix, we explain how we derived the external circuit connected to the solar array coupon. Before arc inception, the surface of the cover glass (dielectric with typically 100-μm thickness) has a positive potential with respect to the underlying cells and the interconnectors, because the coverglass surface has almost the same potential as the plasma although most of the solar array circuit has a negative potential with respect to the plasma. After arcing, the charge stored in the capacitance between the spacecraft and the plasma is discharged and the spacecraft potential increases to near the plasma potential. Then the coverglass surface becomes positive against the plasma. The arc plasma expands from the arc site, neutralizing the charge on the cover glasses. This neutralization of the coverglass charge is observed in the ground tests.[11] A typical satellite of 100-V bus has solar array panels that span longer than 10 m.[13] The 400-V solar array for 1 MW will have a huge number of solar cells and area of the order of 10^3 m^2. The area of the cover glasses (capacitance) will be huge, too. The cover glass supplies a large amount of charge to the arc plasma. It is important to estimate the current waveform supplied from the cover glass before we carry out a test to investigate the cell degradation due to arcing, because the degree of cell damage is likely to depend on the amount of the energy flowing to the arc site. We estimated the current waveform based on Ref. 14.

In Ref. 14, it was observed that the arc plasma could neutralize the charge stored on thin film that simulated cover glass. By data extrapolation, it was concluded that the arc plasma could neutralize the charge of cover glasses within 4 m from the arc site. We assume that the ratio of the neutralized charge to the total charge stored on the cover glasses is 100% at the arc site and decreases linearly to the distance from the arc site, r, untill it becomes 0% at 4 m from the arc site. In short, the charge stored on the cells far from the

arc site remains after arc inception. The velocity of the arc plasma propagating by neutralizing the charge on the cover glass is assumed as 7×10^4 m/s from the experimental results. We also assume the capacitance of the cover glass to be $C_{cg} = 287$ nF/m^2.

We assume that the charge on the cover glass is neutralized radially at the velocity v from the arc site. The charge, $C_{cg}|\Delta V|$, is stored on the cover glass per unit area before arcing, where ΔV is the potential difference between the cover glass and the cell. We denote the fraction of charge neutralized by the expanding plasma as γ_c. We assume that $\gamma_c = 1 - 0.25r$, where r is in meters. We count the time t from the arc inception time. The charge neutralized at r during dt is denoted as dC. From $r = vt$, the discharge current I is

$$I = \frac{\mathrm{d}C}{\mathrm{d}t} = \frac{[\pi(r+dr)^2 - \pi r^2]C_{cg}|V|\gamma_c}{\mathrm{d}t}$$

$$= 2\pi r C_{cg}|V|\gamma_c \frac{\mathrm{d}r}{\mathrm{d}t}$$

$$= 2\pi C_{cg}|V|v^2 t(1 - 0.25vt) \quad \text{(A1)}$$

Substituting the values of C_g, v, and $|V|(= 400$ V) into Eq. (A1), we obtain

$$I = 3.5 \times 10^6 t(1 - 1.8 \times 10^4 t) \quad \text{(A2)}$$

From this equation, the peak of the arc current, I_{max}, is 50 A, and the amount of the charge is 2 mC. Therefore, as the external capacitance we need 5 μF. When we do not connect anything to the external capacitance, the charge stored in the external capacitance flows only though the arc resistance of a few ohms between the solar array and the chamber wall. In such a case, the charge flows instantaneously within a few microseconds and the peak of the current is very large. To match the arc current close to the value denoted in Eq. (A2), we added a resistance and an inductance in series to the capacitance. The experimental circuit is shown in Fig. 4. A voltage of -400 V was applied to the solar array during the experiment. The inductance L and the resistance R are 270 μH and 4.1 Ω, respectively. These values were estimated using a circuit simulator and were corrected slightly via preliminary experiments by trial and error. The waveform of the discharge current measured using this circuit is shown in Fig. 5. In the figure, the estimated current waveform is given by Eq. (A2). The peak of the measured current was 47 A. This value was close to the estimated peak value, 50 A. The amount of charge given by integrating the experimental current in time was 2 mC. Therefore, the entire amount of charge stored in the capacitance was discharged in one pulse.

Acknowledgments

This study is carried out as a part of the Grants-in-Aid for Scientific Research by the Japan Society for the Promotion of Science and the Ground-based Research Announcement for Space Utilization promoted by the Japan Space Forum.

References

[1]Grier, N. T., "Plasma Interaction Experiment II (PIX II): Laboratory and Flight Results," *Spacecraft Environmental Interaction Technology—1983*, NASA CP-2359, 1985, pp. 333–347.

[2]Hastings, D. E., Cho, M., and Kuninaka, H., "The Arcing Rate for a High Voltage Solar Array: Theory, Experiment and Predictions," *Journal of Spacecraft and Rockets*, Vol. 29, No. 4, 1992, pp. 538–554.

[3]Cho, M., Shiraishi, K., Toyoda, K., and Hikita, M., "Basic Developmental Experiment of Arc-Resistive High Voltage Solar Array for Low Earth Orbit," *Journal of the Japan Society of Aeronautical and Space Sciences*, Vol. 50, No. 581, 2002, pp. 215–222.

[4]Toyoda, K., Saionji, A., Cho, M., and Hikita, M., "Experimental Study of Mitigating Arcs on a High Voltage Solar Array in LEO," *Proceedings of the 23rd International Symposium on Space Technology and Science*, JSASS and ISTS, Matsue, Japan, 2002, pp. 379–384.

[5]Jongeward, G. A., Katz, I., Carruth, M. R., Raph, E. L., King, D. Q., and Peterson, T., "High Voltage Solar Arrays for a Direct Drive Hall Effect Propulsion System," *Proceedings of 27th International Electric Propulsion Conference* [CD-ROM], Electric Rocket Propulsion Society, IEPC-01-327, 2001.

[6]Toyoda, K., Matsumoto, T., Cho, M., Nozaki, Y., and Takahashi, M., "Power Reduction of Solar Arrays by Arcing Under Simulated Geosynchronous Orbit Environment," *Journal of Spacecraft and Rockets*, Vol. 41, No. 5, 2004, pp. 854–861.

[7]Katz, I., Davis, V. A., and Snyder, D. B., "Mechanism for Spacecraft Charging Initiated Destruction of Solar Arrays in GEO," AIAA Paper 98-1002, 1998.

[8]Cho, M., Ramasamy, R., Matsumoto, T., Toyoda, K., Nozaki, Y., and Takahashi, M., "Laboratory Tests on 110-Volt Solar Arrays in Simulated Geosynchronous Orbit Environment," *Journal of Spacecraft and Rockets*, Vol. 40, No. 2, 2003, pp. 211–220.

[9]Cho, M., Ramasamy, R., Toyoda, K., Nozaki, Y., and Takahashi, M., "Laboratory Tests on 110-Volt Solar Arrays in Ion Thruster Plasma Environment," *Journal of Spacecraft and Rockets*, Vol. 40, No. 2, 2003, pp. 221–229.

[10]Hayashi, H., Saionji, A., Toyoda, K., Cho, M., and Kuninaka, H., "Development of Plasma Interaction Acceleration Test Facility for Study on Space Material Deterioration," *Proceedings of the 23rd International Symposium Space Technology Science* [CD-ROM], JSASS and ISTS, ISTS 2002-b-28, Matsue, Japan, 2002.

[11]Toyoda, K., Cho, M., and Hikita, M., "Development of Position Identification System of Arc Discharge on a Solar Array in Vacuum by Digital Processing of Video Images," *Journal of the Japan Society of Aeronautical and Space Sciences*, Vol. 51, No. 589, 2003, pp. 82–84.

[12]Saionji, A., Toyoda, K., and Cho, M., "Development of Automatic Data Recording and Analysis System for Laboratory Experiments on High Voltage Solar Array in Space Environment," *Proceedings of Asian Conference on Electrical Discharge and Korea–Japan Symposium on Electrical Discharge and High Voltage Engineering*, IEEJ, Seoul, Republic of Korea, 2002, pp. 63–66.

[13]Leung, P., "Plasma Phenomena Associated with Solar Array Discharges and Their Role in Scaling Coupon Test Results to a Full Panel," AIAA Paper 2002-0628, Jan. 2002.

[14]Cho, M., Miyata, N., Hikita, M., and Sasaki, S., "Discharge over Spacecraft Insulator Surface in Low Earth Orbit Plasma Environment," *IEEE Transactions on Dielectrics and Electrical Insulation*, Vol. 6, No. 4, 1999, pp. 501–506.

I. Boyd
Associate Editor

This article has been cited by:

1. Yalin Wang, Jiandong Wu, Weikang Li, Yi Yin. Space charge measurement of cross-linked polyethylene at low temperatures 180-183. [Crossref]
2. Tatsuo Shimizu, Hiroshi Fukuda, Nguyen Tien Su, Kazuhiro Toyoda, Minoru Iwata, Mengu Cho. 2017. Initial Results From an In-Orbit High-Voltage Experimental Platform: HORYU-IV. *IEEE Transactions on Plasma Science* **45**:8, 1853-1863. [Crossref]
3. Tatsuo Shimizu, Hiroshi Fukuda, Kazuhiro Toyoda, Mengu Cho. 2017. Solar Array Electrostatic Discharge Current and Image Captured in Orbit. *Journal of Spacecraft and Rockets* **54**:2, 497-499. [Citation] [Full Text] [PDF] [PDF Plus]
4. Tatsuo Shimizu, Hiroshi Fukuda, Kazuhiro Toyoda, Mengu Cho. 2015. Development of an In-Orbit High-Voltage Experimental Platform: HORYU-4. *IEEE Transactions on Plasma Science* **43**:9, 3027-3040. [Crossref]
5. Boris Vayner. Possible Decline in Solar Array Performance Due to Electrostatic Discharges in Orbit . [Citation] [PDF] [PDF Plus]
6. Yehia A. Abdel-Aziz, Afaf M. Abd El-Hameed. 2013. Ground-based simulation for the effects of space plasma on spacecraft. *Advances in Space Research* **51**:1, 133-142. [Crossref]
7. Daomin Min, Mengu Cho, Arifur R. Khan, Shengtao Li. 2012. Charge transport properties of dielectrics revealed by isothermal surface potential decay. *IEEE Transactions on Dielectrics and Electrical Insulation* **19**:4, 1465-1473. [Crossref]
8. Teppei Okumura, Mengu Cho, Virginie Inguimbert, Denis Payan, Boris Vayner, Dale C. Ferguson. 2010. International Round-Robin Tests on Solar Cell Degradation Due to Electrostatic Discharge. *Journal of Spacecraft and Rockets* **47**:3, 533-541. [Citation] [PDF] [PDF Plus]
9. Teppei Okumura, Kazuhiro Toyoda, Mengu Cho, Shirou Kawakita, Mitsuru Imaizumi. 2009. Electrostatic Discharge Test on Cu (In, Ga) Se2 Solar Cell Array. *Journal of Spacecraft and Rockets* **46**:5, 999-1006. [Citation] [PDF] [PDF Plus]
10. Teppei Okumura, Kazuhiro Toyoda, Shirou Kawakita, Mitsuru Imaizumi, Mengu Cho. Degradation of Cu(In, Ga)Se<inf>2</inf> thin-film solar cell due to electrostatic discharge 000575-000578. [Crossref]
11. Teppei Okumura, Hirokazu Masui, Kazuhiro Toyoda, Mengu Cho, Kumi Nitta, Mitsuru Imaizumi. 2009. Environmental Effects on Solar Array Electrostatic Discharge Current Waveforms and Test Results. *Journal of Spacecraft and Rockets* **46**:3, 697-705. [Citation] [PDF] [PDF Plus]
12. K. Toyoda, H. Masui, T. Muranaka, M. Cho, T. Urabe, T. Miura, S. Kawakita, Y. Gonohe, T. Kikuchi. 2008. ESD Ground Test of Solar Array Coupons for a Greenhouse Gases Observing Satellite in PEO. *IEEE Transactions on Plasma Science* **36**:5, 2413-2424. [Crossref]
13. Koji Tanaka, Hiroyuki Toyota, Michio Tajima, Susumu Sasaki, Sachiko Katagiri. Basic Experiment of Plasma Interaction with High Voltage Solar Array . [Citation] [PDF] [PDF Plus]
14. Teppei Okumura, Hirokazu Masui, Kazuhiro Toyoda, Mengu Cho, Mitsuru Imaizumi. 2007. Degradation of Electric Performance Due to Electrostatic Discharge on Silicon Solar Cell for Space. *JOURNAL OF THE JAPAN SOCIETY FOR AERONAUTICAL AND SPACE SCIENCES* **55**:647, 590-596. [Crossref]
15. S. Hosoda, T. Okumura, J.-H. Kim, K. Toyoda, M. Cho. 2006. Development of 400 V Solar Array Technology for Low Earth Orbit Plasma Environment. *IEEE Transactions on Plasma Science* **34**:5, 1986-1996. [Crossref]
16. Bryce S. Richards. 2006. Photovoltaics literature survey (no. 43). *Progress in Photovoltaics: Research and Applications* **14**:1, 89-93. [Crossref]